Free-Surface Flow Dynamics and Its Effect on Travel Time Distribution in Unsaturated Fractured Zones - Findings from Analogue Percolation Experiments

Torsten Noffz[1], Jannes Kordilla[1], Marco Dentz[2] and Martin Sauter[1]

[1]University of Göttingen, Dept. of Applied Geology, Germany <torsten.noffz@uni-goettingen.de>

[2] Institute of Environmental Assessment and Water Research (IDAEA), Spanish National Research Council (CSIC), Spain <marco.dentz@csic.es>

I. Introduction

Free-surface flow at fracture intersections

- gravity driven free-surface flow has been identified and described in flow visualization experiments (e.g. Towell (1966); Schmucki (1990); Podgorski (2001))
- experimental approaches using analogue fracture networks suggest the occurrence of versatile flow dynamics during infiltration in the fractured vadose zone (e.g. Dragila (2003, 2004); Glass (2003); Ghezzehei (2005); Nicholl (2005))
- challenges for numerical approaches to recreate flow and transport arise from difficulties in grasping the complexity of non-linear partitioning dynamics at unsaturated fracture intersections

Objective:

- develop and apply methods to accurately delineate droplet and rivulet flow in analogue fracture percolation experiments
- identify the effects of variable flow regimes on mass travel time distribution
- investigate the impacts of variable fracture geometry on partitioning dynamics at unsaturated fracture intersections
- employ an analytical solution proposed by Kordilla et al. (2017) to describe capillary driven fracture inflow

II. Methods

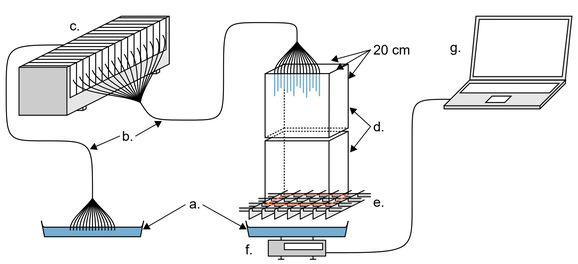

Figure 1: Experimental set-up: a. Water container, b. silicone tubes, c. multichannel dispenser, d. PMMA (poly(methyl methacrylate)) cube ($\theta_0 = (65.2 \pm 2.9)°$), e. coated grate, f. digital balance, and g. computer

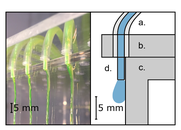

Figure 2: Inlet array consisting of a pre-drilled PMMA board (b.) on top of the upper cube (c.) fixating the silicone tubes (a.) and PTFE (polytetrafluorethylene) outlets (d.)

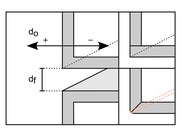

Figure 3: Fracture (left) and cube geometry (right) including variable parameters for aperture width d_f and horizontal offsets of the cubes d_o

III. Delineation of flow regimes

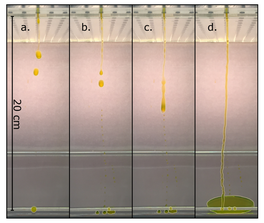

Figure 4: Free surface flow at $Q_0 = 1.5\,\mathrm{ml/min}$ (a.), $2.5\,\mathrm{ml/min}$ (b.,c.), and $3\,\mathrm{ml/min}$ (d.).

Flow rate

- the volumetric flow rate Q_0 is varied to separate continuous droplet ($\leq$ 1.5 ml/min) and rivulet flow ($\geq$ 3 ml/min)

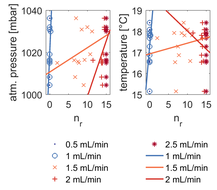

Figure 5: Atm. pressure and temperature vs. average number of stable rivulets n_r produced by 15 inlets. $R^2 = 0.08$ to 0.21 for displayed linear trends.

- the transition is characterized by sliding drops and intermittent rivulets
- a high atm. pressure and temperature seemingly favours the stability of rivulet flow

IV. Partitioning dynamics

1. Single-Inlet

- a sliding drop exhibits complex partitioning phenomena at unsaturated fracture intersections and either bypasses the aperture (a.) or contributes its complete or partial mass to the filling of the fracture (b.-f.)
- a rivulet establishes a hydraulic connection between inlet and fracture while effectively filling it (g.)

Figure 6: Partitioning dynamics at a horizontal fracture intersection captured at 240 fps.

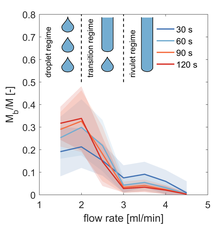

Figure 7: Average mass fractionation M_b/M vs. flow rate for $d_f = 2.5\,\mathrm{mm}$.

- the total liquid mass M can be calculated by

$$M(t) = Q_0 t, \tag{1}$$

where Q_0 $[L^3T^{-1}]$ is the volumetric flow rate. The mass fractionation at time t is given by

$$M(t) = M_f(t) + M_b(t) \tag{2}$$

with M_f being the mass stored in the fracture and M_b representing the bypassing water.

IV. Partitioning dynamics (cont.)

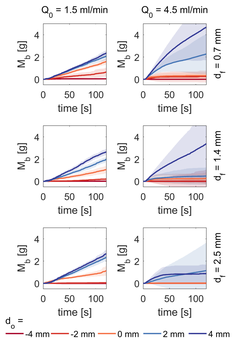

Figure 8: Average M_b vs. time for single-inlet experiments.

- before steady-state conditions are established the contrast of M_b/M is noticeably large for droplet and rivulet flow
- where the horizontal offset d_o is 0 or negative, prevailing droplet flow leads to more fluid bypassing the fracture
- rivulets effectively contribute to its filling
- a small opening width d_f and positive horizontal offsets d_o benefit the mass transport across the aperture

2. Multi-inlet

- equilibrium is reached where the fracture is fully saturated and Q_0 equals the discharge onto the drip pan; M_b rises linearly
- steady-state conditions are successively delayed as the number of fractures n_f and their respective aperture widths d_f increase
- hence, the disparity in bypass efficiency of droplet and rivulet flow is considerably large as long as unsaturated conditions are maintained

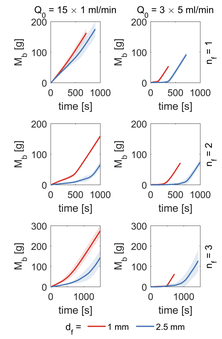

Figure 9: Ensemble means of M_b vs. time for multi-inlet experiments.

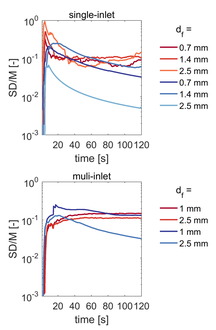

Figure 10: Mean normalized standard deviation of M_b vs. time for droplet (red) and rivulet flow (blue). d_o = 0 mm.

3. Reproducibility

- largest normalized standard deviations can be found for an early stage ($t \leq 30\,\mathrm{s}$) of droplet flow produced by a single inlet
- at an advanced stage SD/M tends to stagnate while not exceeding a value of 0.15
- noise is significantly reduced, where multiple inlets create droplet flow
- during rivulet flow via both inlet conditions, SD/M initially rises and steadily declines throughout the remaining time period

IV. Partitioning dynamics (cont.)

4. Washburn-type fracture inflow

- an analytical solution for capillary driven fracture inflow Q_f following Washburn (1921) is proposed by Kordilla et al. (2017):

The volumetric flow rate Q_0 becomes

$$\frac{dM(t)}{dt} = Q_0 = \frac{dM_f(t)}{dt} + \frac{dM_b(t)}{dt} \tag{3}$$

therefore, the volumetric fracture inflow rate is

$$Q_f(t) = \frac{dM_f(t)}{dt} = Q_0 - \frac{dM_b(t)}{dt}. \tag{4}$$

The penetration length $l(t)$ is obtained by combining Poiseuille's law for planar fractures with an expression for the differential fluid volume in the element of $dl(t)$

$$\frac{dl(t)}{dt} = \frac{c_f}{l(t)}, \tag{5}$$

where the constant c_f is

$$c_f = \frac{\Delta P_c}{\mu} \frac{d_f^2}{4} \tag{6}$$

with μ being the viscosity. The capillary pressure ΔP_c is given by

$$\Delta P_c = \frac{2\sigma cos(\theta)}{d_f}, \tag{7}$$

where σ represents the surface tension and θ being the contact angle. Solving eq. 5 for the initial length $l(t = t_0) = l_0$ gives

$$l(t) = \sqrt{l_0^2 + 2c_f(t - t_0)}. \tag{8}$$

The fluid mass within the fracture is $M_f(t) = A_f l(t)$ for an uniformly advancing front, where A_f is the cross-sectional area of the fracture aperture. Thus, the flow rate into the fracture according to eq. 4 is

$$Q_f(t) = A_f \frac{dl(t)}{dt} = \frac{Q_0}{\sqrt{1 + 2k_f(t - t_0)}} \tag{9}$$

with $A_f c_f = Q_0$ and $k_f = c_f / l_0^2$.

- parameters k_f and t_0 are adjusted in order to match the behaviour of eq. 9 with experimental results

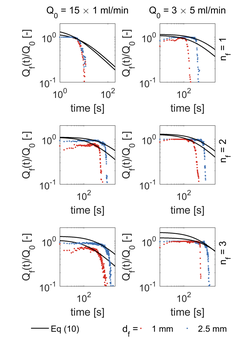

Figure 11: $Q_f(t)/Q_0$ and fitted eq. 9 for multi-inlet experiments

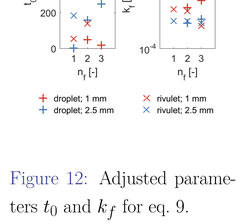

Figure 12: Adjusted parameters t_0 and k_f for eq. 9.

V. Conclusion

- free-surface flow exhibits complex partitioning dynamics at unsaturated fracture intersections with a considerably higher bypass efficiency of droplet flow
- variations of fracture geometry and the extent of the fracture cascade strongly influence the mass travel time distribution
- Washburn-type fracture inflow can be observed and reproduced for both flow regimes by an analytical solution

Outlook:

- results will be applied to validate SPH (smoothed particle hydrodynamics) models of gravity driven free-surface flow
- experimental set-up allows further variation of geometric features as well as the application of geologic materials to account for imbibition with a porous matrix

Acknowledgement:
This work was funded by the Deutsche Forschungsgemeinschaft (DFG; German Research Foundation) under grant no. SA 501/26-1 and KO 53591/1-1.

References:
Washburn (1921): Phys. Rev. **(15(3))**; Towell & Rothfeld (1966): A.I.Ch.E. J. **(12(5))**; Schmucki & Laso (1990): J. of Fluid Mech. **(215)**; Dragila & Weisbrod (2003): Adv. in Water Res. **(26)**; Glass et al. (2003): Water Resour. Res. **(39)**; Dragila & Weisbrod (2004): Water Resour. Res. **(40)**; Ghezzehei (2004): Water Resour. Res. **(40)**; Ghezzehei (2005): Water Resour. Res. **(41)**; Nicholl & Glass (2005): Vad. Zone J. **(4)**; Kordilla (2017): Water Resour. Res. **(in review)**